



# Sensing performance of Fano resonance induced by the coupling of two 1D topological photonic crystals

Zain Elabdeen A. Mohamed<sup>1</sup> · Sayed Elshahat<sup>1</sup> · Alaa M. Abd-Elnaiem<sup>1</sup> · Mohamed Almokhtar<sup>1</sup>

Received: 21 March 2023 / Accepted: 14 June 2023 / Published online: 18 August 2023  
© The Author(s) 2023

## Abstract

In this work, a realized Fano resonance due to the coupling between two 1DTPC is proposed for refractive index sensing with an ultra-high-quality factor of  $10^6$ . The generated Fano can be assigned to the coupling between topological edge states of two 1D TPCs. The resulting Fano peak is characteristic with a high transmission value reach to 99% with high sensing performance parameters making the proposed sensor a novel detector for refractive index. The proposed coupling 1D TPCs show a high sensitivity value of 888.252 nm/RIU, ultra-high-quality factor and figure of merit value reach  $10^6$ , and perfect detection limit value of  $10^{-7}$ . The proposed coupling 1D TPCs provides a straightforward platform for sensing refractive index applications with high performance.

**Keywords** Topological photonic crystal · Fano resonance · The figure of merit · Quality factor

## 1 Introduction

Photonic topological insulators are becoming more and more important in integrated optics because of their unique topologically-protected edge state properties, such as topological protection and immunity to structural disorders (Poshakinskiy et al. 2014; Polini et al. 2013; Lu et al. 2014). To produce topological photonic modes, one-dimensional (1D) optical waveguides and photonic crystals (PCs) (Longhi 2013; Verbin et al. 2013), two-dimensional (2D) rod-based PCs (Dong et al. 2015; Ochiai 2014), three-dimensional (3D) PCs (Lu et al. 2014, 2016), plasmonic nanoparticles (Ling et al. 2015; Poddubny et al. 2014), have all been proposed. The potential uses of topological photonic modes in 2D and 3D topological PCs (TPCs), particularly in the fields of integrated circuits and integrated photonic devices, have been severely constrained due to the challenging design and fabrication. On the other hand, 1D TPCs consisting of multilayers provide straightforward potential in several applications due to their feasible properties such as fast response, high speed, easy design, and fabrication (Sohrabi et al. 2019; Chiasera et al. 2019). Such structures are

---

✉ Zain Elabdeen A. Mohamed  
zain0011@aun.edu.eg

<sup>1</sup> Physics Department, Faculty of Science, Assiut University, Assiut 71516, Egypt

characteristic by inducing robust optical localization resonance mode at topological edge state (TES) with high sensing ability and performance to change in refractive index (RI) (Shen et al. 2016). In the last few years, research focused attention on the change of RI in PCs structures for sensing applications in the field of DNA, cancer cells, bacteria, and gas detections (Dinish et al. 2012; Huang et al. 2011; Fang et al. 2018). Elshahat et al. (2022a) investigated the sensing performance of 1D TPCs for glucose detections by a used structure consisting of multilayers of silicon and silica. In other work, Elshahat et al. (2022b) proposed established TES of 1D TPCs for gas sensing applications with good performance. Recently, Fano resonances have attracted significant attention for use in numerous photonic devices (Breit and Wigner 1936; Adair et al. 1949; Fano 2012), including Fano-transistors (Göres et al. 2000), demultiplexers (Chen et al. 2014), and optical switches (Yu et al. 2014). Fano resonance revealed significant transmission change within a limited wavelength range making it suitable for several applications. As is well known, the interference between the discrete bound state and the continuum of states causes the Fano resonance (Fano 1961). The conventional Fano resonance is fundamentally sensitive to changes in the geometry and environment because it is a resonant scattering state exists by an interference phenomenon between two modes (Limonov 2021). Zangeneh-Nejad and Fleury (2019) investigated the concept of topological Fano resonance for the first time by design and protected from geometry defect. The resulting Fano resonance has a symmetric line shape that is ultra-clear and highly sensitive to external parameters, making it a excellent platform for various applications, particularly in sensors. Geo et al. (2018) construct high Q factor Fano resonance in 1D TPC by coupling between Fabry–Perot mode and topological edge mode. The interference between the topological edge state and bus-waveguide was also used by Gu et al. (2021) to produce Fano resonance. These initiatives open the way for ultra-compact, resilient Fano devices with topological protection, including low-threshold nano lasers, optical switches, and ultra-sensitive optical sensors.

Illuminated by this mechanism, we build a structure based on coupling between two 1D TPCs to generate the Fano resonance response. The first structure consists of five periods and offers a TES, while the other has six periods. This building structure supports a Fano resonance in the optical communication range with a high-quality factor of  $10^6$ , providing the potential in a variety of applications. Through interference coupling between two recently founded TES, our study produces Fano resonances for the first time from two topologies. Therefore, proposed topological photonics could be used more in sensing-related applications. The applications of photonic topological states in integrated photonic devices and information processing chips are also undoubtedly significantly impacted by this.

## 2 Structure and theory

The unit building block of our structure consists of two PCs namely PC1 and PC2 composed of a periodic arrangement of silicon and air layers. Through PC1, the silicon layer has a thickness of  $d_{Si} = 350$  nm, while the air layer has a thickness of  $d_{air} = 300$  nm with lattice constant  $a = 650$  nm as shown in Fig. 1a. Each of the PCs consists of five alternating layers of silicon and air with RI  $n_{Si} = 3.464$  and  $n_{air} = 1$ , respectively. Meanwhile, the layers thickness of PC2 is calculated to be  $d_{Si} = 115$  nm and  $d_{air} = 398$  nm from central wavelength theory (Lam et al. 2005). The transmission spectra of two PCs under applied TE electromagnetic waves are illustrated in Fig. 1b. The black line represented the band

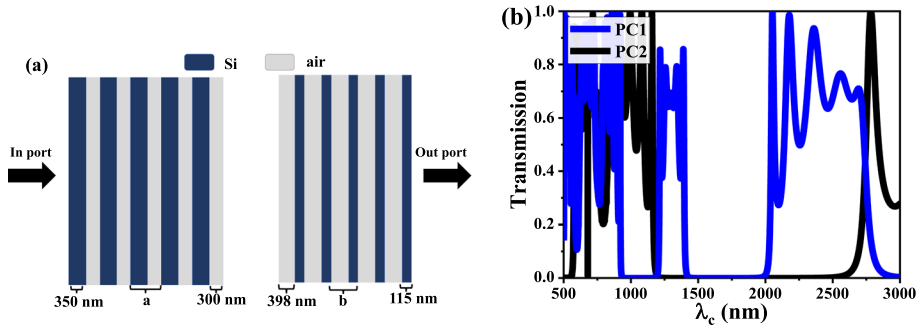


**Fig. 1** **a** Schematic diagrams of PC1 and PC2 composed of five alternative layers of Si and air ( $n_{Si} = 3.464$ ,  $n_{air} = 1$  with  $d_{1Si} = 350$  nm,  $d_{1air} = 300$  nm for PC1, and  $d_{2air} = 398$  nm,  $d_{2Si} = 115$  nm for PC2). **b** The transmission spectra of the two separated PC1 and PC2

gap of PC1 in the range 1390–2052 nm, while the blue color represented the band gap of PC2 in the range 1155–2780 nm. It can be seen that the band gap of PC1 is encompassed in the PC2 band gap. The formed band gap is mainly dependent on the layer's thickness and RI contrast between layers (Mandal and Erickson 2008). Consequently, the two PCs have different topological properties at the same wavelength (Lago et al. 2015). Further, TES can be established at a heterostructure interface between two PCs when stacking together.

The TES is crucial for the study of topological physics for bulk-edge correspondence. While difficult to observe directly, the topological properties of the bulk band can be studied by probing the TES (Hafezi 2014; Hu et al. 2015; Mittal et al. 2016). Although the TES in 2D- and 3D-topological systems can move unidirectionally, this necessitates sophisticated design and manufacturing methods, and hence very few of these structures have a TES that has been empirically detected at optical or communication frequencies (Mittal et al. 2016; Hafezi et al. 2013). The proposed structure is numerically simulated using the finite element method (FEM) in the COMSOL-Multiphysics software, with perfect boundary conditions to absorb electromagnetic (EM) waves around the ports.

### 3 1D TPCs

The schematic diagram of 1D TPCs is illustrated in Fig. 2a resulting from stacking two PCs (PC1 and PC2) and the induced TES appear at wavelength  $\lambda = 1470.350$  nm as shown in Fig. 2b. The zoom-in shape of TES along with a typical Lorentzian fitting, full width at half maximum value ( $FWHM = 22.2$  pm), and transmission value of 95%. From this profound, resonance arises at heterostructure interfaces (Elshahat et al. 2022b; Joannopoulos et al. 2008). For predicting the photonic TES in the 1D PCs heterostructure system, Chan et al. (Xiao et al. 2014) first used the Zak phase (Zak 1989). They provide a convenient approach for building a TES in various 1D PCs heterostructure bandgaps (Gao et al. 2015; Choi et al. 2016; Li et al. 2017). The ability of the edge local TES to induce photons to transmit through the PCs at frequencies in the bandgap provides a novel approach to managing photon transit. The band topological phase, also known as the Zak phase, of the two PCs, however, indicates that the configuration of PC1 differs from the configuration of PC2

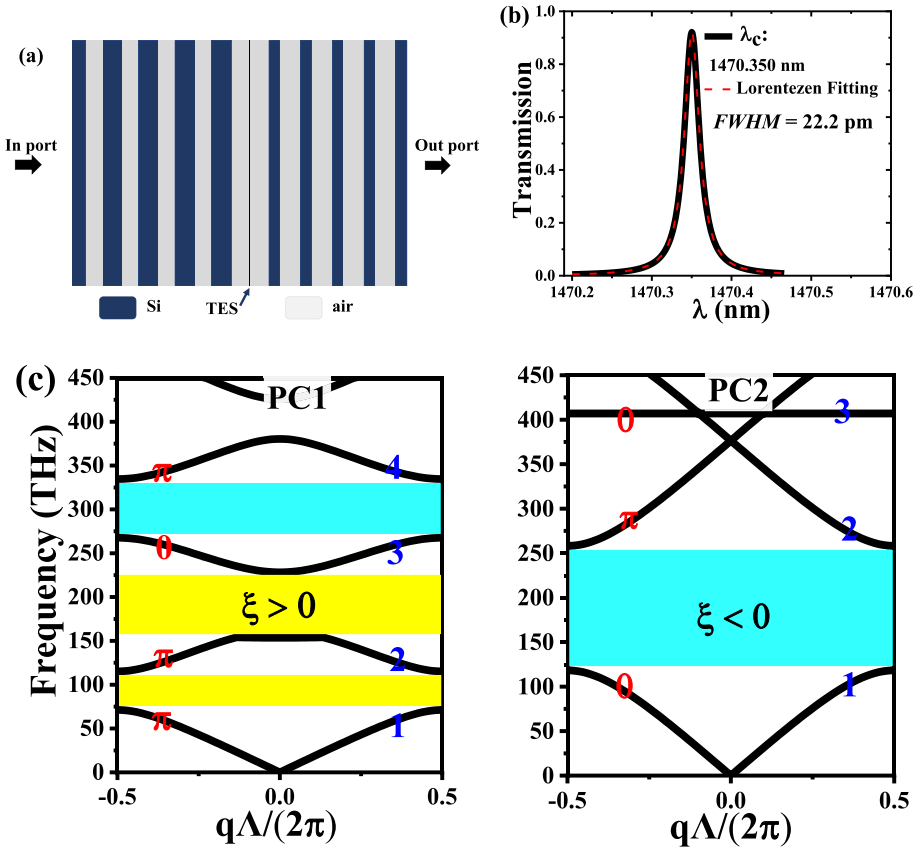


**Fig. 2** a Schematic diagrams of the 1D TPCs structures b the zoom-in of resonance sharp TES peak of 1D TPCs consist of five period and red dashed line with a typical Lorentzian line shape c the band structures for PC1 and PC2 as black curves; and the Zak phase, which is 0 or  $\pi$  for each passband, is labeled in red. (Color figure online)

in terms of topological symmetry. In binary perfect PCs, the  $n$ th band’s Zak phase, which is 0 or  $\pi$ , can be computed using the formula (Xiao et al. 2014).

$$\theta_n^{Zak} = \int_{-\pi/\Lambda}^{\pi/\Lambda} \left[ i \int_{\text{unit cell}} dz \varepsilon(\mathcal{Z}) u_{n,k}^*(\mathcal{Z}) \partial_q u_{n,q}(\mathcal{Z}) \right] dq, \tag{1}$$

In which  $\varepsilon(\mathcal{Z})$  represents the dielectric function,  $u_{n,q}(\mathcal{Z})$  is the periodic-in-cell part of the Bloch electric field eigenfunction of a state on the  $n$ th band with wave vector  $q$ . The straight-forward way to generate an interface state is to construct two PCs, PC1 and PC2, with overlap bandgaps but opposite topological phase bandgap signs. The sum of the Zak phases of all the bands below the  $n$ th gap can be used to establish the topological symmetry sign of the  $n$ th gap as follows:

$$\text{sgn}[\zeta^{(n)}] = (-1)^n (-1)^l \exp\left(i \sum_{m=0}^{n-1} \theta_m^{\text{Zak}}\right), \quad (2)$$

where  $l$  is an integer that denotes how many passband points are crossing under the  $n$ th gap. In the absence of a cross-over,  $l=0$ . The TES manifests at the frequency range of the overlap region when the overlap frequency region of the two gaps of PC1 and PC2 is non-zero and the gap topological invariants of the two PCs have opposite signs. In Fig. 2c, the positive and negative gap topological invariants are denoted by yellow and cyan rectangles, respectively, and the Zak phase of each band is indicated by a blue integer ( $0$  or  $\pi$ ). The Zak phases of the lowest three bands of PC1 are specifically  $\pi$ ,  $\pi$ , and  $0$ , while the lowest three bands of PC2 are  $0$ ,  $\pi$ ,  $0$ . By computing the gap topological invariants of the lowest three gaps, we find that the signs of PC1 gaps are  $+1$ ,  $+1$ ,  $-1$  from low to high frequency, and the signs of PC2 gaps are  $-1$ ,  $+1$ ,  $-1$ , respectively. The TES continue to exist in the second gap of PC1 and the first gap of PC2, which is seen from their differing gap topological symmetries.

The computation of the heterostructure's transmission is shown in Fig. 2b, and it finds transmission peaks at  $\lambda = 1470.350$  nm (corresponding to 204.033 THz) with opposing gap topological invariants of PC1 and PC2. The transmission peak demonstrates that the TES is located at the heterostructure interface of the two PCs, despite being in the bandgap overlap region; the photons were steered through by the TES. The formed TES exhibits good transmission reach to 95% and excellent quality factor ( $Q$ ) that can be defined as the ratio of resonance wavelength to  $FWHM$  thus  $Q = \lambda_r / FWHM = 6.357 \times 10^4$ . The resulting TES with high robustness and  $Q$  factor makes excellent candidates for ultra-sensitive sensors (Elshahat et al. 2022a, 2022b; Weimann et al. 2017). Although TES has a high  $Q$  factor value, it has some issues with transmission value that could limit its use in commercial applications. Our previous work demonstrated the sensing performance of 1D TPCs for gas sensing (Elshahat et al. 2022b). Through this work, the  $Q$  factor value reaches  $6.78 \times 10^5$  and transmission power reaches 90%. The coupling between two 1D PCs is suggested as a way to improve this structure performance for RI sensing applications.

#### 4 The coupling 1D TPCs

The coupling between two 1D TPCs can, as was previously discussed, increase the resonance wavelength caused by TES. Two 1D TPCs are stacked together to form the proposed structure as illustrated in Fig. 3a. The first 1D TPCs structure consists of five periods of PC1 and PC2, while the second one has six periods of them. The differences between the formed TES of the two distinct 1D TPCs structures are shown in Fig. 3b. It can be seen that the transmission and  $FWHM$  values decrease as the structure period increases from five to six. The six period structure provides resonance wavelength at 1470.358 nm with an  $FWHM$  value of about 2.16 pm. On the hand, as seen in Fig. 3c, the Fano resonance peak is formed as a result of the coupling between two TES that result from stacking two 1D TPCs. The generated Fano resonance can be confirmed by computing the electric field distribution as depicted in Fig. 3d. It can be seen that the induced TES mode causes high electric field localization located at the heterostructures interface of two 1D TPCs. In addition, the calculated electric field intensity component vs. arc length, which was obtained by calculating the electric field intensity at each point along a horizontal line going from left

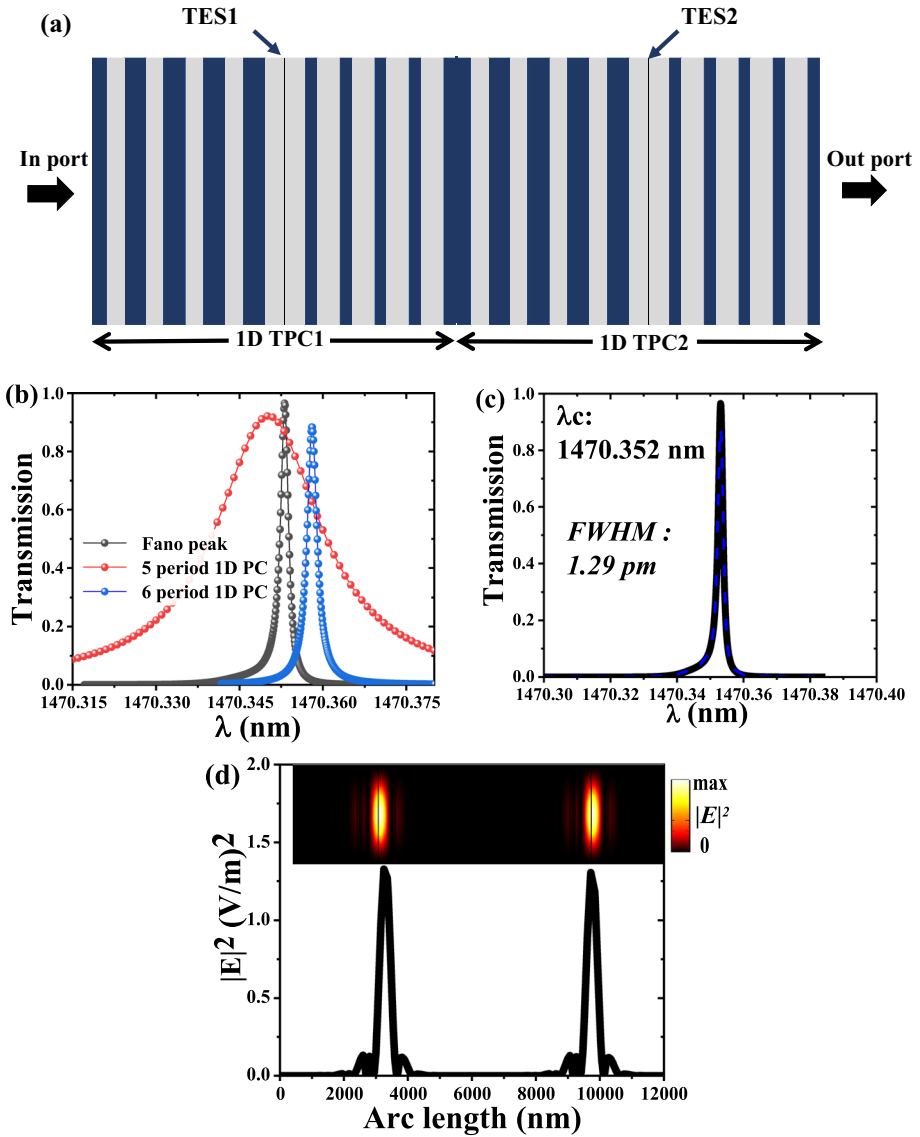


**Fig. 3** **a** Schematic diagram of the proposed structure due to the coupling between two 1D TPCs with a different period **b** the difference between resulting TES in the case of five and six periods and with generated Fano resonance peak. **c** The zoom-in of resonance sharp Fano peak of, in which the fitting curve is represented by a red dashed line with a typical Lorentzian line shape. **d** The calculated electric field  $|E|$  intensity distribution associated with the calculated  $|E|$  inside the proposed coupling 1D TPC heterostructure at the wavelength of the two-interface state. (Color figure online)

to right in the middle of the proposed structure, shows the maximum electric field intensity corresponding to the TES of two structures. Consider the topological Fano resonance produced by the TESs that emerge at the interface of two PCs. The two classes of the resulting edge states are the bright edge state with low-Q originating from the even modes and the

dark edge state with high- $Q$  originating from the bound states in the continuum mode. In this study, the topological Fano resonance is produced by coupling together two 1D TPCs with distinct period values. It is well known that the FWHM decreases, and the  $Q$ -factor rises with an increase in the number of periods via TPCs. As a result, the low period 1D TPC offers low- $Q$  bright edge mode while the high period 1D TPC offers high- $Q$  dark edge mode. Both the bright and dark resonances are topological in nature, and the topological properties of the adjacent bulk insulators are in fact related to the formation of the Fano resonance. A low- $Q$  bright edge mode and a high- $Q$  dark edge mode, which are distinct from trivial cases and typically geometry-sensitive, formed the topological Fano resonance (Zangeneh-Nejad and Fleury 2019). Fano resonance typically improves the sensing performance and quality factor values of any sensor design; this is the main objective of including Fano peaks in our sensor design. The formed Fano peak is shown in Fig. 3c excited at resonance wavelength = 1470.352 nm with FWHM value of (FWHM = 1.29 pm) and transmission power reached 99%. As a result, the proposed structure records a perfect  $Q$  factor value of  $Q = 1.14 \times 10^6$ . When TES of 1D TPCs and generated Fano resonance due to coupling between two TES are compared, the latter has a higher  $Q$  factor and high transmission power. The protected edge state can be used to identify RI changes in structure layers because it has a high transmission spectrum and high  $Q$  factor.

## 5 Sensing performance of coupled 1D TPCs

The sensing mechanism of the proposed coupled 1D TPCs is based on the shift of the resulting Fano resonance peak due to a change in the RI of the air layer through the designed structure. Consequently, the effective RI is changed through the proposed structure and the resulting resonance wavelength of the Fano peak will change (Mandal and Erickson 2008). The resonance condition depends on the difference in refractive indices between silicon and air, as well as the effective index of the proposed structure, which changed as the refractive indices of the air layers changed. The electromagnetics perturbation theory can be used to analyze this phenomenon (Biswas et al. 2018). To verify sensor performance and efficiency there some parameters are determined such as sensitivity ( $S$ ) that can be defined as  $S = \Delta\lambda/\Delta n$  (nm /RIU) (Elshahat et al. 2022a). Where  $\Delta\lambda$  is the change in resonance wavelength of the Fano peak due to a change in RI ( $\Delta n$ ). Sensitivity represents the most widespread way to verify the efficiency of any sensor. Further, the  $Q$  factor and figure of merit ( $FOM$ ) in other parameters to investigate sensor performance and efficiency.  $FOM$  can be expressed as  $FOM = S/FWHM$ , while the  $Q$  factor represented the ratio between resonance wavelength  $\lambda_c$  and FWHM ( $Q = \lambda_c/FWHM$ ). On the other hand, a high transmission value is necessary for a high-performance sensor, which improved due to generated Fano peak than reported 1D TPCs (Elshahat et al. 2022b). Another important factor is the detection limit ( $DL$ ) which can be defined as follows:  $DL = \lambda_c/QS$  (Zhao et al. 2015; White and Fan 2008). The value of  $DL$  means that the sensor can detect a very small change in RI that can be used in various applications with high efficiency. Further parameters to investigated sensing performance of proposed structure is detection accuracy ( $DA$ ) and dynamic range ( $DR$ ) that can be calculated by following relations  $DA = 1/FWHM$ , and  $DR = \lambda_c/\sqrt{FWHM}$  (Almawgani et al. 2023; Taya and Shaheen 2018; Taya 2018). As FWHM get smaller,  $DA$  and  $DR$  value get higher and sensor performance get better. The transmission spectrum of proposed 1D coupled TPCs is illustrated in Fig. 4 at a different

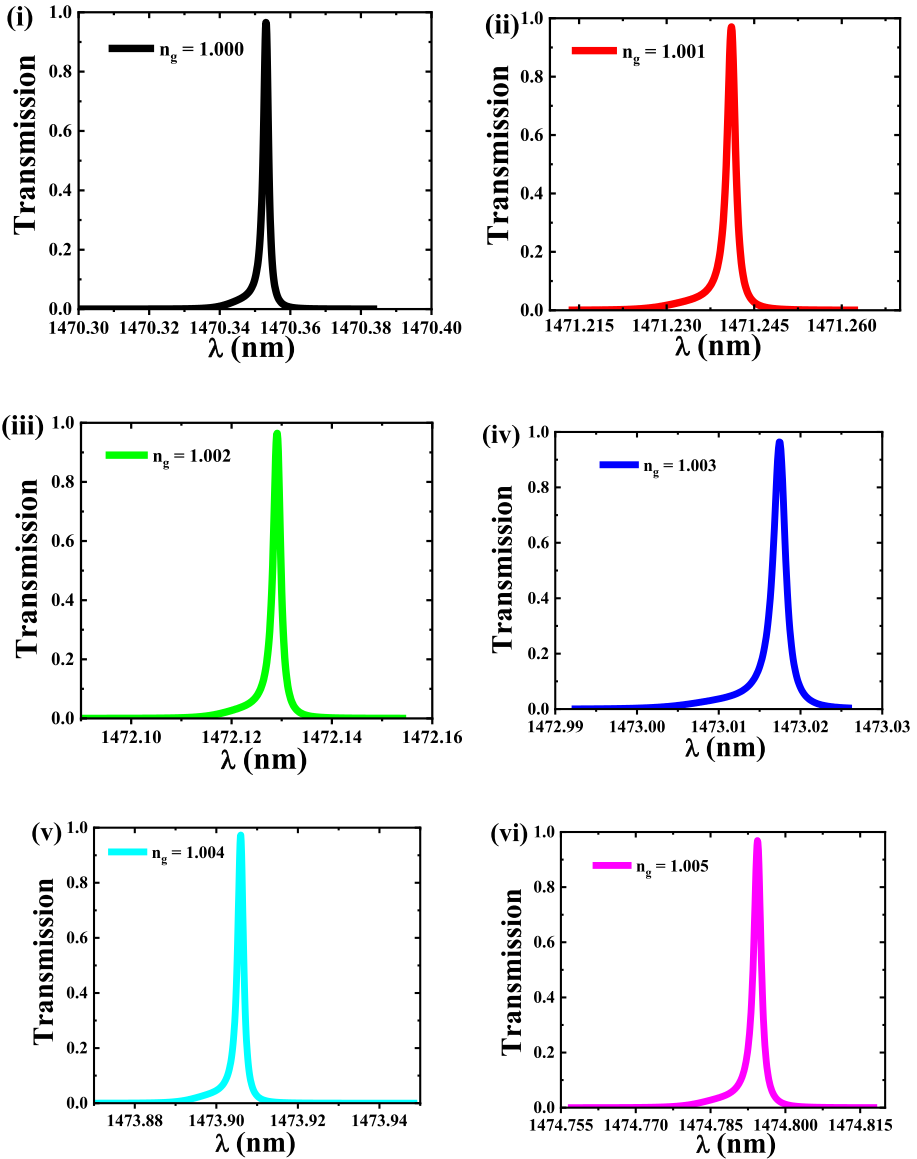


**Fig. 4** The transmission spectrum of proposed coupling 1D TPCs when the RI of the air layers changes from  $i$   $n_{air}=1$  to  $vi$   $n_{air}=1.005$  with an incremental step of 0.001

RI of the air layer ( $n_{air}$ ). It is found that the transmitted peak position shifts toward higher wavelengths (redshift) as the RI of the air layers increases. The Fano resonance wavelength appears at  $\lambda_c = 1470.358$  nm when  $n_{air}=1.000$  with  $FWHM=1.29$  pm, while it shifts to  $\lambda_c = 1470.358$  nm when  $n_{air}$  change to 1.001 with  $FWHM=0.62$  pm.

The investigated value of sensor performance is depicted in Table 1. It can observe that the increase in the RI of the air layers is associated with a redshift in resonance wavelength



**Table 1** The calculated sensing parameters of proposed ID TPCs at RI of air layers

RI	Resonance wave-length (nm)	<i>FWHM</i> (pm)	<i>FOM</i> × 10 <sup>6</sup> ( <i>RIU</i> )	<i>Q</i> × 10 <sup>6</sup>	<i>DL</i> × 10 <sup>-7</sup>
1	1470.35	1.29	–	1.14	–
1.001	1471.24	0.61	1.45	2.41	6.88
1.002	1472.12	0.62	1.43	2.37	6.98
1.003	1473.01	0.62	1.43	2.37	6.99
1.004	1473.90	0.61	1.45	2.40	6.90
1.005	1474.79	0.62	1.42	2.36	7.02

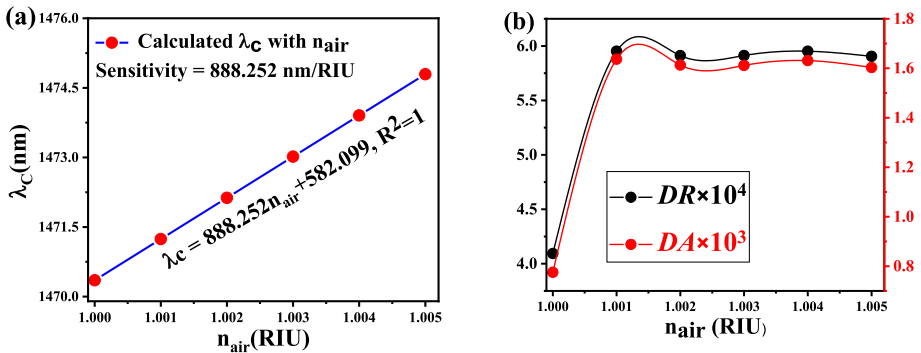


**Fig. 5** **a** The shift in resonance wavelength is a function of change in the RI of air layers, where the red spheres represent simulated results fitting by the solid blue line. **b** The calculated value of *DR* and *DA* of proposed sensor as function of change in RI. (Color figure online)

of the Fano peak and a reduction in *FWHM* value. Consequently, *FOM* and *Q* factor values show little increase with an increase in air layers RI. On the other hand, the proposed structure shows an excellent value of *DL* about  $10^{-7}$ . It is reported that the sensing performance is better with a very tiny *DL* value (Elshahat et al. 2022b). The liner slope between the change in resonance wavelength  $\lambda_c$  vs change in RI  $n_{air}$  can be used to estimate the sensitivity of the proposed structure as displayed in Fig. 5a, where red sphere represented the simulation result fitting by solid blue line ( $S = 888.252$  nm/RIU). In addition, the calculated *Q* factor and *FOM* with extreme value reach  $2.40 \times 10^6$ ,  $1.45 \times 10^6$  RIU with transmission reached 99%. Meanwhile, *DL* with a perfect value of about  $10^{-7}$  RIU. Figure 5b describe the calculated value of *DR* and *DA* of proposed sensor that increase with increase RI. The maximum obtained values of *DR* and *DA* are 59,524.64 and 1631, respectively. The calculated value of *DR* and *DA* confirm high sensing performance of proposed structure when compared with previous work (Almawgani et al. 2023; Taya 2015).

Experimental approaches for the fabrication of PCs layers composed of silicon and air are becoming increasingly popular, as they offer novel insights into the behavior of light. Such layers can be created using a variety of techniques, such as two-photon polymerization, etching of porous silicon, and lithography (Elshahat et al. 2022a, 2022b; Goyal et al. 2016a). Additionally, the use of quantum dots can provide interesting new properties to the PCs layer. The properties of the PCs layer depend on its geometry, so precision is essential when fabricating these layers. Once the layer is created, researchers can study and manipulate the properties of the light, such as its wavelength and intensity. These layers have the potential to revolutionize

**Table 2** Comparison with previously reported PC structures for RI sensing

Reference	$S$ (nm/RIU)	$FOM$ (RIU <sup>-1</sup> )	$DL$ (RIU)	$Q$	T%
Jágorská et al. (2010a)	610	–	$1 \times 10^{-5}$	$2.6 \times 10^4$	99%
Qian et al. (2016)	450	800	$1.6 \times 10^{-4}$	1105	90%
Sansierra et al. (2019)	< 70	1.04	–	–	< 90%
Jágorská et al. (2010b)	510	–	–	$2.6 \times 10^5$	< 90%
Goyal et al. (2016b)	400	8631	–	$3.2 \times 10^5$	–
Elshahat et al. (2022b)	806.658	$3.84 \times 10^5$	$2.60 \times 10^{-6}$	$7.02 \times 10^5$	90%
This work	888.252	$1.45 \times 10^6$	$7.02 \times 10^{-7}$	$2.40 \times 10^6$	99%

a wide range of applications, from data transmission and optoelectronics to solar cells and displays. Table 2 illustrates the comparison between our work and the literature. One or more of the sensing parameters, such as  $S$ ,  $FOM$ , or  $Q$ , was weak in the earlier work. Through this work, a great foundation has been established for constructing topological photonic sensors. The heterostructure described here with the Fano resonance peak will provide excellent candidates for the development of topological photonic devices. In comparison to existing published RI sensors including gas sensors, the suggested sensor is characterized by simple fabrication.

## 6 Conclusion

In conclusion, Fano resonance was realized in 1D TPCs heterostructure for refractive index sensing with a high-quality factor of  $10^6$ . The study shows the resulting coupling between the TES of two 1D TPCs composed of different periods of silicon and air layers. The sensing performance of designed coupling 1TPCs was investigated by replacing air layer RI from 1 to 1.005 with constant step 0.001. The proposed structure shows excellent sensing parameters represented in  $S=888.252$  nm/RIU,  $Q > 10^6$ ,  $FOM > 10^6$  RIU, and a perfect value of detection limit of  $10^{-7}$  RIU. The generated Fano resonance with a high transmission value of about 99% in optical communication provides a novel sensor for refractive index sensing.

**Author contributions** ZM: conceived the idea, checked the simulation results, and revised the manuscript. ZM: performed the simulations and prepared the draft. ZM: discussed the results and checked the draft. ZM: discussed the results and revised the manuscript. The author read and approved the final manuscript.

**Funding** Open access funding provided by The Science, Technology & Innovation Funding Authority (STDF) in cooperation with The Egyptian Knowledge Bank (EKB). The authors did not receive any funds to support this research.

**Availability of data and materials** The data that support the findings of this study are available from the corresponding author upon reasonable request.

## Declarations

**Competing interests** The authors declare that they have no known competing financial interests or personal relationships that could have appeared to influence the work reported in this paper.

**Open Access** This article is licensed under a Creative Commons Attribution 4.0 International License, which permits use, sharing, adaptation, distribution and reproduction in any medium or format, as long as you give appropriate credit to the original author(s) and the source, provide a link to the Creative Commons licence, and indicate if changes were made. The images or other third party material in this article

are included in the article's Creative Commons licence, unless indicated otherwise in a credit line to the material. If material is not included in the article's Creative Commons licence and your intended use is not permitted by statutory regulation or exceeds the permitted use, you will need to obtain permission directly from the copyright holder. To view a copy of this licence, visit <http://creativecommons.org/licenses/by/4.0/>.

## References

- Adair, R., Bockelman, C., Peterson, R.: Experimental corroboration of the theory of neutron resonance scattering. *Phys. Rev.* **76**(2), 308 (1949)
- Almawgani, A.H., et al.: A photonic crystal based on porous silicon as a chemical sensor for the detection of methanol compound. *Indian J. Phys.*, 1–10 (2023)
- Biswas, S., Guin, S., Das, N.R.: Photonic crystal for gas sensing application. In: *Advances in Computer, Communication and Control: Proceedings of ETES 2018*, 2019, pp. 459–467: Springer
- Breit, G., Wigner, E.: Capture of slow neutrons. *Phys. Rev.* **49**(7), 519 (1936)
- Chen, Z., Hu, R., Cui, L., Yu, L., Wang, L., Xiao, J.: Plasmonic wavelength demultiplexers based on tunable Fano resonance in coupled-resonator systems. *Opt. Commun.* **320**, 6–11 (2014)
- Chiasera, A., et al.: Coherent emission from fully Er<sup>3+</sup> doped monolithic 1-D dielectric microcavity fabricated by rf-sputtering. *Opt. Mater.* **87**, 107–111 (2019)
- Choi, K.H., Ling, C., Lee, K., Tsang, Y.H., Fung, K.H.: Simultaneous multi-frequency topological edge modes between one-dimensional photonic crystals. *Opt. Lett.* **41**(7), 1644–1647 (2016)
- Dallago, V., Atala, M., FoaTorres, L.E.F.: Floquet topological transitions in a driven one-dimensional topological insulator. *Phys. Rev. A* **92**(2), 023624 (2015)
- Dinish, U., Fu, C.Y., Soh, K.S., Ramaswamy, B., Kumar, A., Olivo, M.: Highly sensitive SERS detection of cancer proteins in low sample volume using hollow core photonic crystal fiber. *Biosens. Bioelectron.* **33**(1), 293–298 (2012)
- Dong, J.-W., et al.: Conical dispersion and effective zero refractive index in photonic quasicrystals. *Phys. Rev. Lett.* **114**(16), 163901 (2015)
- Elshahat, S., Mohamed, Z.E.A., Almokhtar, M., Lu, C.: High tunability and sensitivity of 1D topological photonic crystal heterostructure. *J. Opt.* **24**(3), 035004 (2022a)
- Elshahat, S., Mohamed, Z.E.A., Abd-Elnaiem, A.M., Ouyang, Z., Almokhtar, M.: One-dimensional topological photonic crystal for high-performance gas sensor. *Micro Nanostruct.* **172**, 207447 (2022b)
- Fang, Y., Li, X., Xia, J., Xu, Z.: Sensing gases by the pole effect of parity-time symmetric coupled resonators. *IEEE Sens. J.* **19**(7), 2533–2539 (2018)
- Fano, U.: Effects of configuration interaction on intensities and phase shifts. *Phys. Rev.* **124**(6), 1866 (1961)
- Fano, U.: *Atomic collisions and spectra*. Elsevier, (2012)
- Gao, W.S., Xiao, M., Chan, C.T., Tam, W.Y.: Determination of Zak phase by reflection phase in 1D photonic crystals. *Opt. Lett.* **40**(22), 5259–5262 (2015)
- Gao, W., et al.: Fano-resonance in one-dimensional topological photonic crystal heterostructure. *Opt. Express* **26**(7), 8634–8644 (2018)
- Göres, J., et al.: Fano resonances in electronic transport through a single-electron transistor. *Phys. Rev. B* **62**(3), 2188 (2000)
- Goyal, A.K., Dutta, H.S., Singh, S., Kaur, M., Husale, S., Pal, S.: Realization of large-scale photonic crystal cavity-based devices. *J. Micro/nanolithogr. MEMS MOEMS* **15**(3), 031608–031608 (2016a)
- Goyal, A.K., Dutta, H.S., Pal, S.: Performance optimization of photonic crystal resonator based sensor. *Opt. Quant. Electron.* **48**(9), 1–11 (2016b)
- Gu, L., et al.: Fano resonance from a one-dimensional topological photonic crystal. *APL Photon.* **6**(8), 086105 (2021)
- Hafezi, M.: Measuring topological invariants in photonic systems. *Phys. Rev. Lett.* **112**(21), 210405 (2014)
- Hafezi, M., Mittal, S., Fan, J., Migdall, A., Taylor, J.: Imaging topological edge states in silicon photonics. *Nat. Photon.* **7**(12), 1001–1005 (2013)
- Hu, W., Pillay, J.C., Wu, K., Pasek, M., Shum, P.P., Chong, Y.: Measurement of a topological edge invariant in a microwave network. *Phys. Rev. X* **5**(1), 011012 (2015)
- Huang, C.-S., et al.: Application of photonic crystal enhanced fluorescence to cancer biomarker microarrays. *Anal. Chem.* **83**(4), 1425–1430 (2011)
- Jágerská, J., Zhang, H., Diao, Z., Le Thomas, N., Houdré, R.: Refractive index sensing with an air-slot photonic crystal nanocavity. *Opt. Lett.* **35**(15), 2523–2525 (2010b)

- Jágerská, J., Le Thomas, N., Zhang, H., Diao, Z., Houdre, R.: Refractive index gas sensing in a hollow photonic crystal cavity. In: 2010a 12th International Conference on Transparent Optical Networks, 2010a, pp. 1–4: IEEE
- Joannopoulos, J., Johnson, S.G., Winn, J.N., Meade, R.D.: Photonic Crystals: Molding the Flow of Light, p. 305 (2008)
- Lam, W., Chu, L., Wong, C., Zhang, Y.: A surface plasmon resonance system for the measurement of glucose in aqueous solution. *Sens. Actuators B Chem.* **105**(2), 138–143 (2005)
- Li, C., Hu, X., Yang, H., Gong, Q.: Unidirectional transmission in 1D nonlinear photonic crystal based on topological phase reversal by optical nonlinearity. *AIP Adv.* **7**(2), 025203 (2017)
- Limonov, M.F.: Fano resonance for applications. *Adv. Opt. Photon.* **13**(3), 703–771 (2021)
- Ling, C., Xiao, M., Chan, C.T., Yu, S.F., Fung, K.H.: Topological edge plasmon modes between diatomic chains of plasmonic nanoparticles. *Opt. Express* **23**(3), 2021–2031 (2015)
- Longhi, S.: Zak phase of photons in optical waveguide lattices. *Opt. Lett.* **38**(19), 3716–3719 (2013)
- Lu, L., Joannopoulos, J.D., Soljačić, M.: Topological photonics. *Nat. Photon.* **8**(11), 821–829 (2014)
- Lu, L., Fang, C., Fu, L., Johnson, S.G., Joannopoulos, J.D., Soljačić, M.: Symmetry-protected topological photonic crystal in three dimensions. *Nat. Phys.* **12**(4), 337–340 (2016)
- Mandal, S., Erickson, D.: Nanoscale optofluidic sensor arrays. *Opt. Express* **16**(3), 1623–1631 (2008)
- Mittal, S., Ganeshan, S., Fan, J., Vaezi, A., Hafezi, M.: Measurement of topological invariants in a 2D photonic system. *Nat. Photon.* **10**(3), 180–183 (2016)
- Ochiai, T.: Broken symmetry and topology in photonic analog of graphene. *Int. J. Mod. Phys. B* **28**(02), 1441004 (2014)
- Poddubny, A., Miroshnichenko, A., Slobozhanyuk, A., Kivshar, Y.: Topological Majorana states in zigzag chains of plasmonic nanoparticles. *ACS Photon.* **1**(2), 101–105 (2014)
- Polini, M., Guinea, F., Lewenstein, M., Manoharan, H.C., Pellegrini, V.: Artificial honeycomb lattices for electrons, atoms and photons. *Nat. Nanotechnol.* **8**(9), 625–633 (2013)
- Poshakinskiy, A., Poddubny, A., Pilozzi, L., Ivchenko, E.: Radiative topological states in resonant photonic crystals. *Phys. Rev. Lett.* **112**(10), 107403 (2014)
- Qian, X., Zhao, Y., Zhang, Y.-N., Wang, Q.: Theoretical research of gas sensing method based on photonic crystal cavity and fiber loop ring-down technique. *Sens. Actuators B Chem.* **228**, 665–672 (2016)
- Sansierra, M.C., Morrone, J., Cornacchiulo, F., Fuertes, M.C., Angelomé, P.C.: Detection of organic vapors using tamm mode based devices built from mesoporous oxide thin films. *ChemNanoMat* **5**(10), 1289–1295 (2019)
- Shen, H., Wang, Z., Wu, Y., Yang, B.: One-dimensional photonic crystals: fabrication, responsiveness and emerging applications in 3D construction. *RSC Adv.* **6**(6), 4505–4520 (2016)
- Sohrabi, F., Hamidi, S.M., Asgari, N., Ansari, M.A., Gachiloo, R.: One dimensional photonic crystal as an efficient tool for in-vivo optical sensing of neural activity. *Opt. Mater.* **96**, 109275 (2019)
- Taya, S.A.: Theoretical investigation of slab waveguide sensor using anisotropic metamaterial. *Opt. Appl.* **45**(3), 405–417 (2015)
- Taya, S.: Ternary photonic crystal with left-handed material layer for refractometric application. *Opto-Electron. Rev.* **26**(3), 236–241 (2018)
- Taya, S.A., Shaheen, S.A.: Binary photonic crystal for refractometric applications (TE case). *Indian J. Phys.* **92**(4), 519–527 (2018)
- Verbin, M., Zilberberg, O., Kraus, Y.E., Lahini, Y., Silberberg, Y.: Observation of topological phase transitions in photonic quasicrystals. *Phys. Rev. Lett.* **110**(7), 076403 (2013)
- Weimann, S., et al.: Topologically protected bound states in photonic parity–time-symmetric crystals. *Nat. Mater.* **16**(4), 433–438 (2017)
- White, I.M., Fan, X.: On the performance quantification of resonant refractive index sensors. *Opt. Express* **16**(2), 1020–1028 (2008)
- Xiao, M., Zhang, Z., Chan, C.T.: Surface impedance and bulk band geometric phases in one-dimensional systems. *Phys. Rev. X* **4**(2), 021017 (2014)
- Yu, Y., et al.: Fano resonance control in a photonic crystal structure and its application to ultrafast switching. *Appl. Phys. Lett.* **105**(6), 061117 (2014)
- Zak, J.: Berry's phase for energy bands in solids. *Phys. Rev. Lett.* **62**(23), 2747 (1989)
- Zangeneh-Nejad, F., Fleury, R.: Topological fano resonances. *Phys. Rev. Lett.* **122**(1), 014301 (2019)
- Zhao, Y., Zhang, Y.-N., Wang, Q., Hu, H.: Review on the optimization methods of slow light in photonic crystal waveguide. *IEEE Trans. Nanotechnol.* **14**(3), 407–426 (2015)